Engineering Dynamic Structural Color Pixels at Microscales by Inhomogeneous Strain-Induced Localized Topographic Change

Yujie Ke,[1,2] Qifeng Ruan,[1,3] Yanbin Li,[4] Hao Wang,[1] Hongtao Wang,[1] Wang Zhang,[1] Chengfeng Pan,[1] Parvathi Nair Suseela Nair,[1,2] Jie Yin,[4] Joel K. W. Yang [1,2]*

1. Engineering Product Development, Singapore University of Technology and Design, Singapore 487372, Singapore.

2. Institute of Materials Research and Engineering (IMRE), Agency for Science, Technology and Research (A*STAR), 2 Fusionopolis Way, Innovis #08-03, Singapore 138634, Republic of Singapore

3. Ministry of Industry and Information Technology Key Lab of Micro-Nano Optoelectronic Information System, Harbin Institute of Technology (Shenzhen), Shenzhen 518055, P. R. China.

4. Department of Mechanical and Aerospace Engineering, North Carolina State University, Raleigh, NC, 27695, USA.

[*]Corresponding author: Joel K. W. Yang (joel_yang@sutd.edu.sg).

KEYWORDS

Mechanochromics, Two-Photon Lithography, Dynamic Structural Color, Reconfigurable Structures, Nanoscale 3D Printing

ABSTRACT

Structural colors in homogeneous elastomeric materials predominantly exhibit uniform color changes under applied strains. However, juxtaposing mechanochromic pixels that exhibit distinct responses to applied strain remains challenging, especially at microscales where the demand for miscellaneous spectral information increases. Here, we present a method to engineer microscale switchable color pixels by creating localized inhomogeneous strain fields at the level of individual micro-lines. Trenches produced from transfer casting from 2.5D structures into elastomers exhibit a uniform structural color in the unstretched state due to interference and scattering effects, while show different colors under an applied uni-axial strain. This programmable topographic change resulting in color variation arises from strain mismatch between layers and trench width. We utilized this effect to achieve the encryption of text strings with Morse code. The effective and facile design principle is promising for diverse optical devices based on dynamic structures and topographic changes.

MAIN TEXT

Structural-color materials exhibit vivid colors by manipulating the incident light through delicate nano/micro-structures.[1-4] Colors are generated due to physical effects, e.g. interference in multilayered thin films or cavities,[5-7] Bragg diffraction in photonic crystals,[8, 9] plasmonic resonances in metallic nanostructures,[3, 10] and Mie resonances in high-reflective-index dielectric nanomaterials.[8, 11] There is a long-standing vigorous research interesting to tune the structural color dynamically,[12-16] Particularly, the dynamic control of color through mechanical deformation,[6, 17-24] also called mechanochromics, has being attracted increasing interest due to its great potential in strain/pressure sensors for emerging research topics of healthcare and robotics,[6, 25, 26] as well as in camouflage,[19] and information storage.[27]

Developing strain-responsive pixels is an effective way to render more information than static color pixels. The most common method to achieve color pixels is to change the geometric design parameters, e.g., lattice constant.[28, 29] This method has been applied for dynamic plasmonic color,[10, 14] wrinkle colors,[30] 1D-to-3D photonic crystals,[8, 19] and height-dependent interference.[27] However, the change of such parameters commonly produces color pixels that are easily distinguished in the initial state, which is a drawback for information encryption. Another widely used method is to integrate responsive structural-coloring materials with programmable actuators, and each actuator acts as an individual color pixel. However, this method usually produces relatively large pixels, e.g., ~1-5 mm^2 on inflating panels[19] and ~100 μm^2 on microelectromechanical systems.[31] These big pixels significantly reduce the information density carried by colors, and further miniaturizing pixels will greatly complicate the actuator system. So far, the method to solve these two problems is rarely reported, and it is still challenging to produce smaller pixels (sub-pixels) that only show up color differences under strain.

Recent investigations show that the method to introduce pre-designed patterns is effective to locally control various deformations to make reconfigurable structures.[32, 33] The concept of reconfigurable structures is known for their subtle local structural designs, such as Kirigami,[32] Origami,[33] and interweaving metastructure[34] which have been applied in soft-electronics,[35] actuators,[36] and energy-saving windows.[37] These structures are based on the design principle of creating localized inhomogeneous strain fields by, such as strain mismatch and/or versatile structural patterns.[32, 38, 39] This principle is largely unexplored in previous works of structural colors, and is promising to solve the abovementioned problems by producing mechanochromic sub-pixels under global deformation.

In this work, by applying the principle of creating localized inhomogeneous strain fields, we present a facile design to achieve juxtaposing mechanochromic pixels that show distinct responses to global stress. We demonstrate the method on a single micron-sized trench, a newly introduced building block in structural colors.[27, 40] The trench is made in polydimethylsiloxane (PDMS) with a crust of oxidized PDMS. By controlling the localized width, the trench shows the same colors in the unstretched state but exhibits a series of pixels of different colors in the stretched state. We demonstrate that the color originates from depth-dependent constructive interference across the visible spectrum, and the pixel emergence in the stretched trench is due to local variations in topography. The samples are durable, and their serial nature is fitting for conveying cyphertext as demonstrated using Morse code.

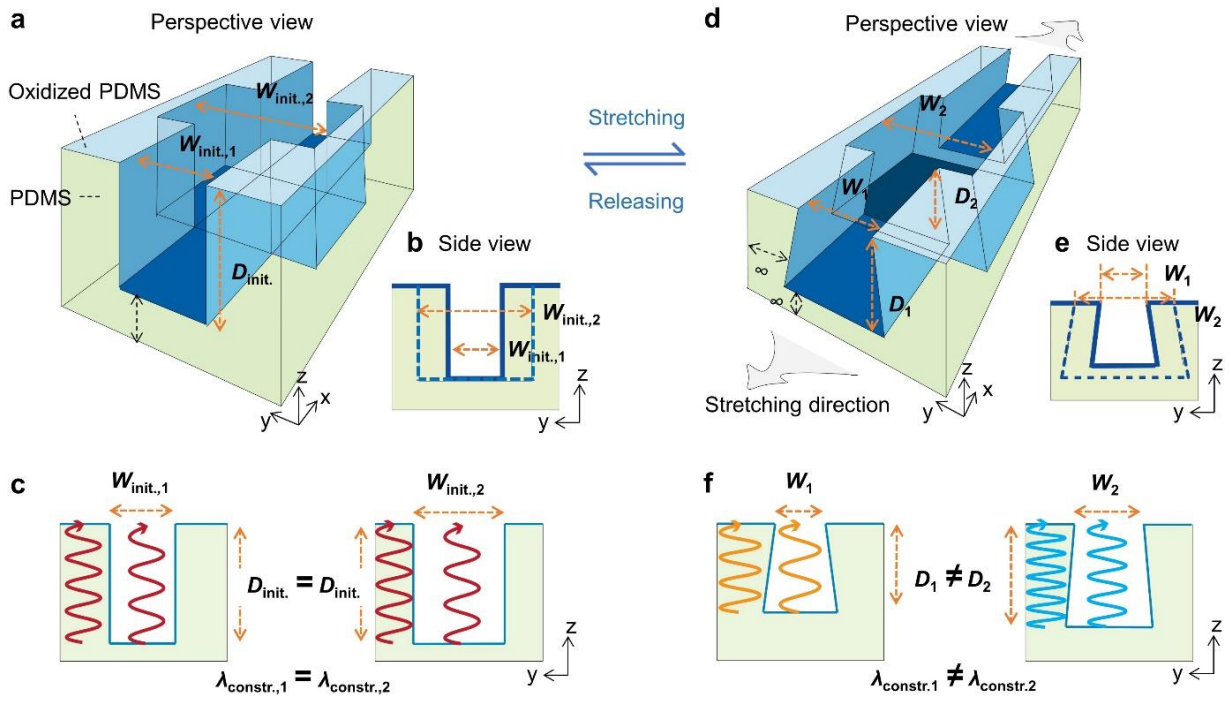

Figure 1. Design and working mechanism. (a) Schematics of the perspective and (b) side (y-z) views of a representative color pixel design on a single trench in an unstretched (initial) state. (c) Cross-sectional view of trenches in an unstretched state with different widths ($W_{init,1}$ and $W_{init,2}$) showing constructive interference of transmitted light. The constructive wavelength is the same for these two cross-sections as the trenches are of equal depth ($D_{init.}$). (d) The perspective and (e) side view of the design schematic when stretched along the x-axis (the stretched state) resulting in varying depths. (f) Constructive interference now occurs at different wavelengths for the trenches having different depths (D_1 and D_2).

The photonic line is designed to be a trench structure with a uniform width ($W_{init,1}$) and depth (D_{init}), made of PDMS (Figure 1a). To realize the strain-responsive color pixel, a thin stiff crust of oxidized PDMS and a different trench width ($W_{init,2}$) are introduced to generate deformed structural difference under uni-axial stretching along x-axis (Figure 1a). In the side-view, the color pixel and photonic line show the same trench structure with a uniform D_{init} but different widths ($W_{init,1}$ and

$W_{init,2}$) (Figure 1b). When the incident light transmits through the structure alone in its z direction, the light goes through the PDMS and the air gap, inducing constructive/destructive interference right above the top surface. The constructive interference forms only when the light wavelength matches its traveling distance (depth).[27] The initial state is defined as the unstretched state. On the state, the line and pixel with the D_{init} generate a constructive interference for light with the same wavelength, illustrated by red as an example in Figure 1c.

Upon uni-axially stretching the PDMS trench along the length becomes elongated along the x-axis (length) and shrunk along both the y- (width) and z-axis (depth) due to the Poisson's effect (Figure 1d). During the shrinking process, the width plays an important role to affect the shrinkage ratio, resulting in different depths in trapezoidal cross-sections with different widths: D_1 in W_1 section and D_2 in W_2 section. As seen from the side-view illustration (Figure 1e), both sections show a smaller opening than the initial state, and they are different from each other in width and depth. Specifically, this difference makes the constructive interference different: Incident light with wavelength $\lambda_{constr.,1}$ (e.g. indicated in orange) forms constructive interference through D_1, while the light with another wavelength $\lambda_{constr.,2}$ (e.g. indicated in blue) forms the interference through a larger depth of D_2 (Figure 1f). This effect results in different colors for the W_2 (the pixel) and W_1 section (the trench). Thus, a strain-responsive color pixel forms on a stretched state only.

To understand how trenches deform upon stretching, we conducted finite element method (FEM) analysis. In the simulation, two trenches are set with the same D_{init} of 3.2 μm but different W_{init} = 1.8 or 4.0 μm (Figure 2a). The oxidized PDMS crust is set with a modulus of 100 MPa, a thickness of 30 nm, and a Poisson's ratio of 0.36.[41] We captured the cross-section strain contours during the stretching process that shows the transition from rectangular to a trapezoidal cross-section under increasing strain (Figure 2a).

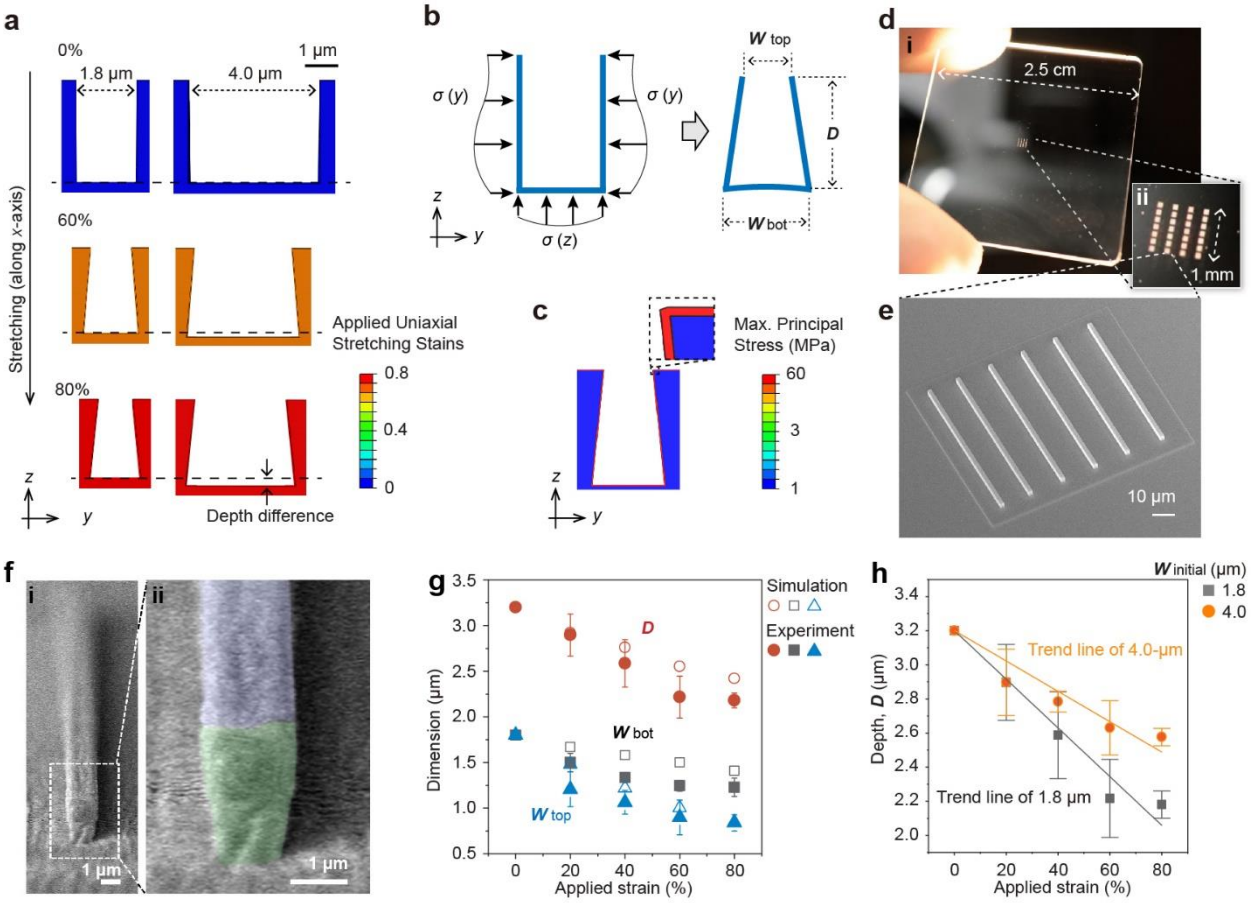

Figure 2. Structure analysis. (a) Calculated strain contour of the cross-section structure under an increasing strain from 0% to 80%. (b) Illustration of the simplified beam model to analyze the structure change. (c) The principle stress contour of the 60%-stretched sample on its cross-section. (d) Photo image of the produced mold on a 2.5 x 2.5 cm quartz substrate (i) and its zoom-in photo of the 4x7 write field array (ii). (e) Tilt-view SEM image of a representative writing field containing 6 lines with a width of 1.8 μm. (f) Tilt-view SEM image of a replica cross-section for the 1.8-μm sample under 60% strain (i), and its zoom-in image (ii). (g) Experimental and calculated analysis of the D, W_{top}, and $W_{bot.}$ for the 1.8-μm trench sample under a stain of 0% to 80%. (h) Experimental analysis of the W_{init} effect on D under increasing strains. The two trend lines by linear fitting highlight the D changes of 1.8-μm and 4.0-μm W_{init} trenches.

This shape change is induced by the large stiffness mismatch between the oxidized PDMS crust (E_t) and the PDMS substrate (E_s) with $E_t >> E_s$. Significant inhomogeneous strain fields will generate in the two different layers. Simplifying the crust into a simple beam model (Figure 2b), the deflections of its side parts can be generally expressed as

$$A(z) = \int_{bot}^{top} \frac{\sigma(y)}{EI} dz \qquad (1)$$

where A(z) is deflection amplitude, $\sigma(y)$ is the effective normal stress applied on the side part generated from the inhomogeneous strain field, and EI is the bending stiffness. Given the obvious lateral (along y direction) resistance from the bottom part of the cross section, the top end of the side part can deform more easily to exhibit larger deflections than the bottom end with $A_{bottom} > A_{top}$. Consequently, rather than uniformly deforming as rectangulars on the design without the crust (Figure S1), the cross section of crusted sample deforms into a trapezoid shape (Figure 2a and 2b). This shape change is directly observed and reflected on the stress contour of the 60%-strained sample, where significantly higher stress on the stiff crust compared with the soft PDMS matrix (Figure 2c). The cross-section shape is analyzed by three parameters of W_{top}, W_{bot}, and D in the following analysis (Figure 2b).

More importantly, we found that the 4.0-μm trench is deeper than the 1.8-μm trench under the same x-directional stretching strain (Figure 2a). This is further analyzed using numerical simulations, showing that a cross-section with a shorter width is pushed higher by the PDMS substrate with a larger stress (Figure. S2). This depth difference is important to affect the transmittance interference, which will be discussed in the following section.

In the experiment, a 3D-printing combined with a molding process is applied to produce the PDMS trench followed by an O_2-plasma (60 s and 100 W) process to get the oxidized PDMS crust (Figure S3). The mold is produced on a quartz substrate, shown as the tiny white patch in Figure 2d i,

which contains 4x7=28 write fields (Figure 2d ii), and each write field contains 6 convex lines (Figure 2e and Figure S4). The PDMS samples deform significantly under vacuum in scanning electron microscope (SEM) measurement (Figure S5), so we conduct the shape measurement by again molding the concave structure and measuring its convex replica (Figure S6). The tile-view SEM image is captured for the replica of the sample (W_{init} of 1.8 μm and D_{init} of 3.2 μm) under an applied strain of 60% (Figure 2f i), and the sample is found to have a trapezoid cross-section (Figure 2f ii). We analyzed the three shape parameters of the sample under the applied strain of 20%-80% using the same method and compared the result with the simulation. It is demonstrated that all the W_{top}, W_{bot}, and D decrease under increasing strain (structure shrinking) (Figure 2g). Besides, the W_{top} decreases much more significantly than the W_{bot}, suggesting the gradual shape change from a rectangular to trapezoid change (Figure 2g). The experiment analysis is consistent with the simulation (Figure 2g), indicating the validity of the analysis method.

More importantly, it is found that tuning the W_{init} is effective to control the D during the stretching process. The sample with a W_{init} of 1.8 μm (named 1.8-μm sample) has a D of ~2.2 μm under 60% strain, which is ~0.4 μm less than the 4.0-μm sample (Figure 2h). In other words, the 1.8-μm sample shows a larger D decreasing trend than 4.0-μm one (the two trend lines in Figure 2h), suggesting that the trench with a relatively narrow W is less resistant to shrink during the stretching process. The effect of W_{init} to D under stretching states and the shape change to trapezoid are demonstrated on the samples with W_{init} ranging from 1.6 to 4.0 μm (Figure S7).

We further analyze the strain effect on the optical property of trenches. It is observed that all trenches show gradual color change under the stretching along the length direction. In the 1.8-μm sample, the color changes from red on 0% strain, blue on 30% strain, to magenta on 80% strain (Figure 3a). It is observed a transmittance peak, defined as 1st peak in Figure 3b, shows a blue shift

from ~635 nm on 0% strain, to ~480 nm on 30% strain, and to ~465 nm on 60% strains(Figure 3b). The strain-induced blue shift is consistent with the simulation result (Figure 3c and S8) based on the abovementioned structure geometry calculations (Figure 2g).

Moreover importantly, all trenches with W_{init} from 1.4 to 4.0 μm show the same red on unstretched states, while having colors different from each other under stretched states (Figure 3a). A gradual color gradient is observed from purple to blue on 60%-strained samples with increasing W_{init} from 1.4 to 4.0 μm (Figure 3a). On unstretched states, all trenches show two transmittance peaks located at ~430 and ~630 nm, respectively (Figure 3d). However, in the 60% state, the trenches are characterized by different peak positions, and a red shift of the 1st peak is observed under increasing W_{initl} (Figure 3e). All trenches start with the same color while changing differently during the stretching process, indicating the validity to differentiate colors in stretching only by adjusting the W_{init}, a geometry parameter that gives negligible effect to the initial color but significantly affects the trecnch shape deformation under global stretching. Besides, it is worth mentioning that the red color is observed to be a single line for a narrow trench (e.g. W_{init} = 1.4 μm) and to be two parallel lines for a wide trench (e.g. W_{init} = 4.0 μm) (Figure 3a), suggesting the constructive interference forms near the side areas with abrupt height difference. The principle, by tuning the W_{init} to generate color difference under stretching, is also applicable to trenches with different D_{init} (Figure S9).

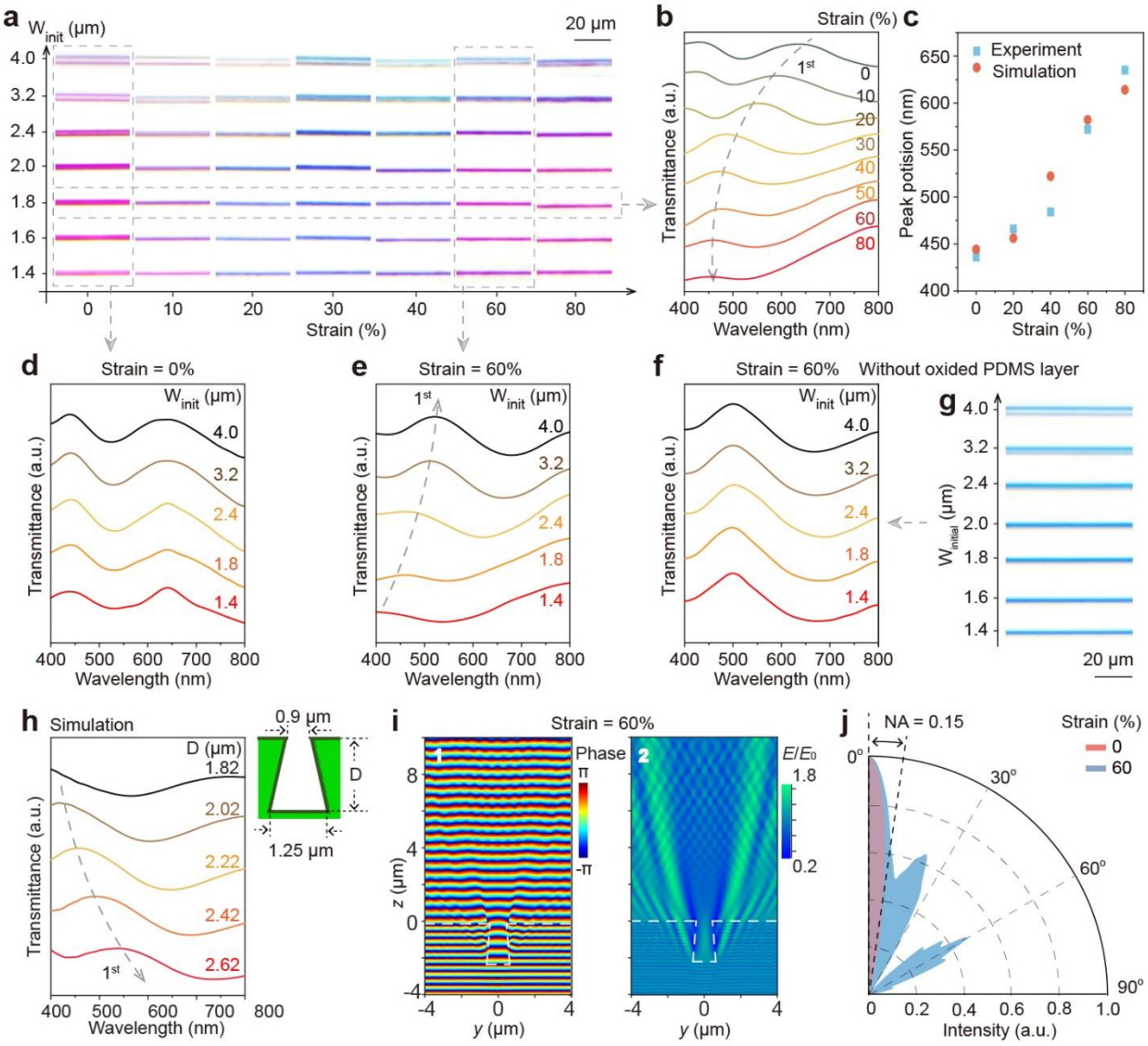

Figure 3. Optical and spectral analysis. (a) Transmission optical microscopy images of the trench samples with different W_{init} (1.4 to 4.0 μm) under variable strains (0% to 80%). (b) Transmittance spectra of the 1.8-μm trench sample under the increasing strains. (c) Analysis of experimental and calculated 1st peak positions under variable strains. (d, e) Transmittance spectra of the trenches with W_{init} of 1.4-4.0 μm under the applied strain of 0% (d) and 60% (e). (f) Transmittance spectra of trenches without the crust on their 60% stretching states, and (g) their corresponding transmission optical microscopy images. (h) Simulated transmittance spectra of the trapezoid

shape with a variable D and a fixed W_{top} and W_{bot} of 0.9 and 1.25 μm, respectively. (i) Calculated near-field electrical phase (1) and amplitude (2) at the wavelength of 513 nm on the cross-sections of the stretched (60% strain) sample. (f) Normalized far-field angular projections of TE-mode transmission light of 513 nm for unstretched and stretched samples.

It is also found that the oxidized PDMS crust plays an important role to generate this color difference. Without the O-plasma treatment, the trenches with different W_{init} are measured to have the same peak position (Figure 3f) and the same color (Figure 3g) under 60% strains. Tuning the oxygen-plasma duration is also found to be an effective way to modulate the peak position and colors under a certain strain (Figure S10). The oxygen-plasma treatment is reported to effectively oxidized the PDMS surface,[41] and Young's modulus and hardness are increased by prolonging duration or promoting power.

To understand the effect of depth and side-wall profile on the spectral response, we simulated the effects of varying the geometric parameters D, W_{bot}, W_{top} on the transmittance spectrum. We chose parameter values close to the 60%-stretched state. It is found that increasing D from 1.82 to 2.62 μm (keeping W_{bot} and W_{top} at 1.25 and 0.9 μm, respectively) leads to a spectral redshift of more than 140 nm (Figure 3h). The side wall effect is investigated by changing the W_{top} (0.5-1.4 μm) or W_{bot} (0.65-1.55 μm) (keeping D at 2.22 μm). These side-wall variations induce peak shifts of less than 30 nm (Figure S11). The result shows that D plays the dominant role in spectral shift compared to changes in the side-wall profile.

The trench structure can be simplified as a binary phase grating of air and PDMS, and the transmittance phase difference is:

$$\Delta\varphi = \frac{2\pi D\,(n_{\mathrm{PDMS}} - n_{\mathrm{air}})}{\lambda} \qquad (2)$$

where n is the refractive index, D is the trench depth, and λ is the wavelength. Constructive interference forms with a certain λ matching to the structure geometry D, resulting when $\Delta\varphi$ matches an even integer of π:

$$i = \frac{\Delta\varphi}{\pi} \qquad (3)$$

where when i of even integer leads to a maximum transmittance and is shown as the peak position of λ in the transmittance spectrum. Taking the i to be 4, the peak positions are calculated to be 462 and 672 nm for 60% and 0% strained samples, respectively, which are consistent with the measured spectra. Slight differences can be attributed to the n difference of the thin crust and some cracks may form on the stretching states, which is not considered in the simplified model and is challenging to be measured accurately in quantity.

To understand the scattering pattern of the trapezoid cross-section, the simulated near-field electric field amplitude and phase are illustrated on 60% stretched 1.8-μm sample at the wavelength of 513 nm (Figure 3i). The electric vector is perpendicular to the PDMS trench, defined as TE mode. The phase speeds inside PDMS substrate and the air gap are different (Figure 3i 1), leading to a redistribution of light intensity after passing through the single PDMS trench (Figure 3i 2). Besides, the scattering at the wavelength of 513 nm mainly goes forward within a wider angle than the unstretched state (Figure S12), which shows negligible side scattering lobes. In a 60% stretched state, the side wall of the trench is titled with a narrower exit, inducing strong side scattering in the far field (Figure 3j), which is outside of the collecting angle 8.6° of the objective lens. The TM mode shows a similar result (Figure S13). The variation of scattering mode changes the collected energy ratio between different wavelengths, hence the spectrum, i.e., color is changed.

Moreover, the 1.8-μm sample shows no decay under the stretching-releasing cycling tests (within 100 cycles) or after a storing of up to 6 months (Figure S14). This is attributed to the simplicity of

the design configuration made of PDMS, which is physically durable and oxidization resistant.[42-44] In addition, the molding process is reliable and reusable, and the first 10 PDMS replicas using a mold exhibit similar performance (Figure S14).

In addition, we investigated the effect of density of trenches by changing the separation (4 to 14 μm) between neighboring trenches (Figure S15a). As the depths of the trenches were identical, we observed that all samples exhibit similar colors and transmittance spectra in their initial state (Figure S15b). When strained by 60% these trenches exhibit distinct colors in their stretched states (Figure S15c). Only samples with large separations (14 μm) show a similar appearance to the abovementioned individual trench, as the large spectral blueshift of ~200 nm as indicated by the arrows produces similar spectra in both states. The phenomenon is much different from our previous work,[27] where all samples perform similarly to individual trenches regardless of the periodicity during the stretching process. We conducted the FEM simulation to understand this effect. It is found that the separation is effective to control the geometry of trapezoid cross-section: the reduction in depth is less for the case of trenches with a small separation (4 μm) than the case with a big separation (14 μm) in the 60%-stretched state (Figure S15d), and the 14-μm sample shows a similar geometry to the individual trench. The result suggests a critical separation ≥14-μm is essential for trenches to perform individually, and a separation smaller than 14 μm tends to make the trenches more resistant to deformation, thus affecting the optical property.

We further demonstrate that the pixel design principle is capable of encoding information that can be easily machine-read. Here we present an example to encode and decode the word "UNIVERSITY" using the International Morse code. The demo is made on 1.6-μm trenches with uniform *D* of 3.2 μm, and the Morse characters of "•" and "▬" are designed as the 2.4-μm pixels on a length of 4 and 12 μm, respectively (Figure 4a). A produced mold is illustrated in Figure S16.

The produced samples show a uniform red in unstretched states (Figure 4b), while the change to lines with alternative patterns of magenta and violet under 60% elongating (Figure 4c). These blue patterns can be read out based on the length of the violet pixels to give a character's pattern (Figure 4d), which can be translated by the International Morse code (Figure 4e) to decode the target words information of "UNIVERSITY" successfully (Figure 4f). Slightly

More importantly, we demonstrate that multiple sets of information can be encoded by introducing three different W_{init} (1.6, 2.4, and 4.0 μm) based on the same coding method. We design the three sets of colorful Morse code by three different W_{init} of 1.6, 2.4, and 4.0 μm, and distinguished the "•" and "▬" by different lengths of 6 and 12 μm (Figure 4g). The sample shows a uniform red color on initial states while switching to juxtaposing mechanochromic pixels under 60% strain (Figure 4h). Though slightly non-uniform deformations and color variations are observed at the inter-pixel regions (Figure S17), the pixels can be read out by distinguishing their colors to be magenta, violet, and azure blue. Then, the three sets can be translated via Morse codes to get information of "MECHANOCHROMIC STRUCTURAL COLOR PIXEL" for magenta, "NANOPHOTONICS AND NANOFABRICATION" for violet, and "ENGINEERING PRODUCT DEVELOPMENT PILLAR" for azure blue (Figure 4i). Moreover, we demonstrate this process is machine-readable with an average accuracy of 93%, which is ~96%, ~90%, and 96% for magenta, violet, and azure blue, respectively (Figure S18).

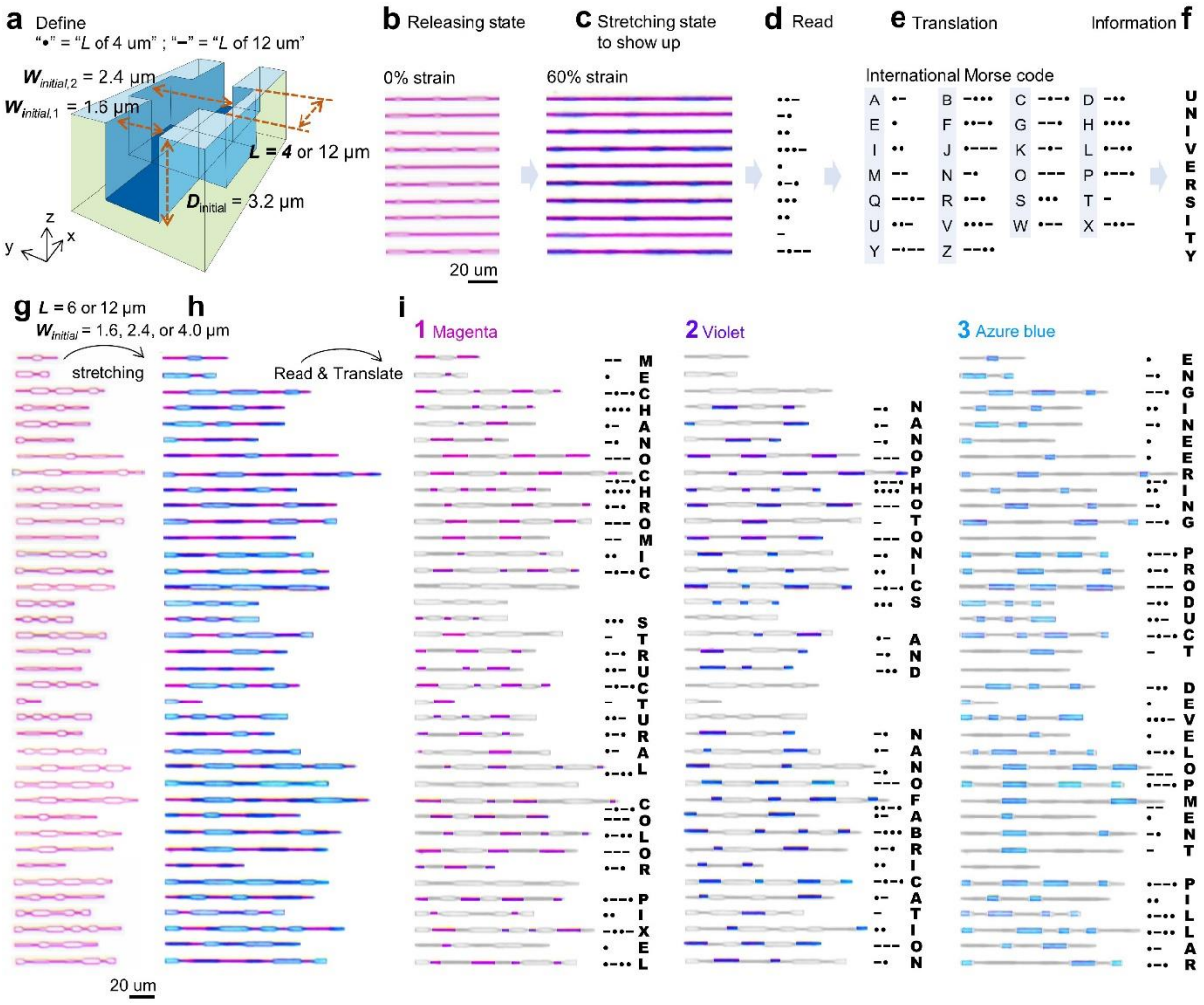

Figure 4. Demonstration of the Morse code cyphertext. (a-f) Example showing the coding of the word "UNIVERSITY". (a) Structure design. (b) The optical microscope image of the design in its unstretched state (b) and 60%-strained state (c). (d) Readout patterns based on the magenta color pixels in the stretched state. (e) Translation process by referring to the International Morse code. (f) Encryption information was obtained. (g-i) The demo encodes 3 sets of information. (g-h) The microscopy image of the produced sample in its unstretched state (g) and 60%-stretching state (h). (i) Readout and translation processes to obtain the 3 sets of information by distinguishing the color patterns.

In summary, we demonstrate a method to engineer the local structural colors in elastomeric materials under global strains. The principle is to create localized inhomogeneous strain fields by strain mismatch and structural parameter variation. We prove the principle on a single trench line made of PDMS and oxidized crust. By adjusting the localized width, the line exhibits a uniform color in the original states, while changing to pixelated chains under stretching. The color change is proven due to the depth-dependent constructive interference, and the localized width is proved to effectively control the depth on stretching states only. The produced sample is durable and is capable to encode multiple sets of texts into color information through the International Morse code. The work provides a facile method to produce mechanochromic color pixels on a microscale, and the principle is promising for diverse optical devices based on material topography.

ASSOCIATED CONTENT

Supporting Information

The Supporting Information is available free of charge at

Experimental methods and additional figures as described in the text (PDF)

AUTHOR INFORMATION

Corresponding Author

Joel K. W. Yang - Engineering Product Development, Singapore University of Technology and Design, Singapore 487372, Singapore; Institute of Materials Research and Engineering (IMRE), Agency for Science, Technology and Research (A*STAR), 2 Fusionopolis Way, Innovis #08-03, Singapore 138634, Republic of Singapore; Email: joel_yang@sutd.edu.sg.

Authors

Yujie Ke - Engineering Product Development, Singapore University of Technology and Design, Singapore 487372, Singapore; Institute of Materials Research and Engineering (IMRE), Agency for Science, Technology and Research (A*STAR), 2 Fusionopolis Way, Innovis #08-03, Singapore 138634, Republic of Singapore.

Qifeng Ruan - Engineering Product Development, Singapore University of Technology and Design, Singapore 487372, Singapore; Ministry of Industry and Information Technology Key Lab of Micro-Nano Optoelectronic Information System, Harbin Institute of Technology (Shenzhen), Shenzhen 518055, P. R. China.

Yanbin Li - Department of Mechanical and Aerospace Engineering, North Carolina State University, Raleigh, NC, 27695, USA.

Hao Wang - Engineering Product Development, Singapore University of Technology and Design, Singapore 487372, Singapore.

Hongtao Wang - Engineering Product Development, Singapore University of Technology and Design, Singapore 487372, Singapore.

Wang Zhang - Engineering Product Development, Singapore University of Technology and Design, Singapore 487372, Singapore.

Chengfeng Pan - Engineering Product Development, Singapore University of Technology and Design, Singapore 487372, Singapore.

Parvathi Nair - Engineering Product Development, Singapore University of Technology and Design, Singapore 487372, Singapore.

Jie Yin - Department of Mechanical and Aerospace Engineering, North Carolina State University, Raleigh, NC, 27695, USA.

Notes

The authors declare no competing financial interest.

ACKNOWLEDGMENT

Joel K. W. Yang thanks to the funding support by National Research Foundation (NRF) Singapore, under its Competitive Research Programme NRF-CRP001-021 and CRP20-2017-0004, as well as NRF Investigatorship Award NRFNRFI06-2020-0005.

REFERENCES

(1) Daqiqeh Rezaei, S.; Dong, Z.; You En Chan, J.; Trisno, J.; Ng, R. J. H.; Ruan, Q.; Qiu, C.-W.; Mortensen, N. A.; Yang, J. K. W., Nanophotonic Structural Colors. *ACS Photonics* **2021,** *8*, 18-33.

(2) Parton, T. G.; Parker, R. M.; van de Kerkhof, G. T.; Narkevicius, A.; Haataja, J. S.; Frka-Petesic, B.; Vignolini, S., Chiral self-assembly of cellulose nanocrystals is driven by crystallite bundles. *Nat. Commun.* **2022,** *13*, 2657.

(3) Kumar, K.; Duan, H.; Hegde, R. S.; Koh, S. C. W.; Wei, J. N.; Yang, J. K. W., Printing colour at the optical diffraction limit. *Nat. Nanotechnol.* **2012,** *7*, 557-561.

(4) Wang, H.; Ruan, Q.; Wang, H.; Rezaei, S. D.; Lim, K. T. P.; Liu, H.; Zhang, W.; Trisno, J.; Chan, J. Y. E.; Yang, J. K. W., Full Color and Grayscale Painting with 3D Printed Low-Index Nanopillars. *Nano Lett.* **2021,** *21*, 4721-4729.

(5) Ito, M. M.; Gibbons, A. H.; Qin, D.; Yamamoto, D.; Jiang, H.; Yamaguchi, D.; Tanaka, K.; Sivaniah, E., Structural colour using organized microfibrillation in glassy polymer films. *Nature* **2019,** *570*, 363-367.

(6) Miller, B. H.; Liu, H.; Kolle, M., Scalable optical manufacture of dynamic structural colour in stretchable materials. *Nat. Mater.* **2022**, *21*, 1014-1018.

(7) Goodling, A. E.; Nagelberg, S.; Kaehr, B.; Meredith, C. H.; Cheon, S. I.; Saunders, A. P.; Kolle, M.; Zarzar, L. D., Colouration by total internal reflection and interference at microscale concave interfaces. *Nature* **2019,** *566*, 523-527.

(8) Yang, W.; Xiao, S.; Song, Q.; Liu, Y.; Wu, Y.; Wang, S.; Yu, J.; Han, J.; Tsai, D.-P., All-dielectric metasurface for high-performance structural color. *Nat. Commun.* **2020,** *11*, 1864.

(9) Wu, P.; Wang, J.; Jiang, L., Bio-inspired photonic crystal patterns. *Mater. Horiz.* **2020,** *7*, 338-365.

(10) Kristensen, A.; Yang, J. K. W.; Bozhevolnyi, S. I.; Link, S.; Nordlander, P.; Halas, N. J.; Mortensen, N. A., Plasmonic colour generation. *Nat. Rev. Mater.* **2016,** *2*, 16088.

(11) Dong, Z.; Ho, J.; Yu, Y. F.; Fu, Y. H.; Paniagua-Dominguez, R.; Wang, S.; Kuznetsov, A. I.; Yang, J. K. W., Printing Beyond sRGB Color Gamut by Mimicking Silicon Nanostructures in Free-Space. *Nano Lett.* **2017,** *17*, 7620-7628.

(12) Neubrech, F.; Duan, X.; Liu, N., Dynamic plasmonic color generation enabled by functional materials. *Sci Adv.* **2020**, *6*, eabc2709.

(13) Ge, J.; Yin, Y., Responsive Photonic Crystals. *Angew. Chem. Int. Ed.* **2011,** *50*, 1492-1522.

(14) Duan, X.; Kamin, S.; Liu, N., Dynamic plasmonic colour display. *Nat. Commun.* **2017,** *8*, 14606.

(15) Wang, G.; Chen, X.; Liu, S.; Wong, C.; Chu, S., Mechanical Chameleon through Dynamic Real-Time Plasmonic Tuning. *ACS Nano* **2016,** *10*, 1788-1794.

(16) Shao, L.; Zhuo, X.; Wang, J., Advanced Plasmonic Materials for Dynamic Color Display. *Adv. Mater.* **2018,** *30*, 1704338.

(17) Zhang, C.; Jing, J.; Wu, Y.; Fan, Y.; Yang, W.; Wang, S.; Song, Q.; Xiao, S., Stretchable All-Dielectric Metasurfaces with Polarization-Insensitive and Full-Spectrum Response. *ACS Nano* **2020,** *14*, 1418-1426.

(18) Zhou, Q.; Park, J. G.; Bae, J.; Ha, D.; Park, J.; Song, K.; Kim, T., Multimodal and Covert–Overt Convertible Structural Coloration Transformed by Mechanical Stress. *Adv. Mater.* **2020,** *32*, 2001467.

(19) Kim, S. U.; Lee, Y. J.; Liu, J.; Kim, D. S.; Wang, H.; Yang, S., Broadband and pixelated camouflage in inflating chiral nematic liquid crystalline elastomers. *Nat. Mater.* **2022,** *21*, 41-46.

(20) Zhang, W.; Wang, H.; Wang, H.; Chan, J. Y. E.; Liu, H.; Zhang, B.; Zhang, Y.-F.; Agarwal, K.; Yang, X.; Ranganath, A. S.; Low, H. Y.; Ge, Q.; Yang, J. K. W., Structural multi-colour invisible inks with submicron 4D printing of shape memory polymers. *Nat. Commun.* **2021,** *12*, 112.

(21) Kose, O.; Tran, A.; Lewis, L.; Hamad, W. Y.; MacLachlan, M. J., Unwinding a spiral of cellulose nanocrystals for stimuli-responsive stretchable optics. *Nat. Commun.* **2019,** *10*, 510.

(22) Liang, H.-L.; Bay, M. M.; Vadrucci, R.; Barty-King, C. H.; Peng, J.; Baumberg, J. J.; De Volder, M. F. L.; Vignolini, S., Roll-to-roll fabrication of touch-responsive cellulose photonic laminates. *Nat. Commun.* **2018,** *9*, 4632.

(23) Chen, Y.; Duan, X.; Matuschek, M.; Zhou, Y.; Neubrech, F.; Duan, H.; Liu, N., Dynamic Color Displays Using Stepwise Cavity Resonators. *Nano Lett.* **2017,** *17*, 5555-5560.

(24) Li, J.; Chen, Y.; Hu, Y.; Duan, H.; Liu, N., Magnesium-Based Metasurfaces for Dual-Function Switching between Dynamic Holography and Dynamic Color Display. *ACS Nano* **2020,** *14*, 7892-7898.

(25) Quan, Y. J.; Kim, Y. G.; Kim, M. S.; Min, S. H.; Ahn, S. H., Stretchable Biaxial and Shear Strain Sensors Using Diffractive Structural Colors. *ACS Nano* **2020,** *14*, 5392-5399.

(26) Fu, F.; Shang, L.; Chen, Z.; Yu, Y.; Zhao, Y., Bioinspired living structural color hydrogels. *Sci. Rob.* **2018,** *3*, eaar8580.

(27) Ruan, Q.; Zhang, W.; Wang, H.; Chan, J. Y. E.; Wang, H.; Liu, H.; Fan, D.; Li, Y.; Qiu, C. W.; Yang, J. K. W., Reconfiguring Colors of Single Relief Structures by Directional Stretching. *Adv. Mater.* **2022,** *34*, e2108128.

(28) Hou, J.; Li, M.; Song, Y., Patterned Colloidal Photonic Crystals. *Angew. Chem. Int. Ed.* **2018,** *57*, 2544-2553.

(29) Cho, Y.; Lee, S. Y.; Ellerthorpe, L.; Feng, G.; Lin, G.; Wu, G.; Yin, J.; Yang, S., Elastoplastic Inverse Opals as Power-Free Mechanochromic Sensors for Force Recording. *Adv. Funct. Mater.* **2015,** *25*, 6041-6049.

(30) Wu, K.; Zhu, T.; Zhu, L.; Sun, Y.; Chen, K.; Chen, J.; Yuan, H.; Wang, Y.; Zhang, J.; Liu, G.; Chen, X.; Sun, J., Reversible Mechanochromisms via Manipulating Surface Wrinkling. *Nano Lett.* **2022,** *22*, 2261-2269.

(31) Han, Z.; Frydendahl, C.; Mazurski, N.; Levy, U., MEMS cantilever-controlled plasmonic colors for sustainable optical displays. *Sci Adv* **2022,** *8*, eabn0889.

(32) Tang, Y.; Lin, G.; Yang, S.; Yi, Y. K.; Kamien, R. D.; Yin, J., Programmable Kiri-Kirigami Metamaterials. *Adv. Mater.* **2017,** *29*, 1604262.

(33) Cui, J.; Poblete, F. R.; Zhu, Y., Origami/Kirigami-Guided Morphing of Composite Sheets. *Adv. Funct. Mater.* **2018,** *28*, 1802768.

(34) Ke, Y.; Li, Y.; Wu, L.; Wang, S.; Yang, R.; Yin, J.; Tan, G.; Long, Y., On-Demand Solar and Thermal Radiation Management Based on Switchable Interwoven Surfaces. *ACS Energy Lett.* **2022,** *7*, 1758-1763.

(35) Rogers John, A.; Someya, T.; Huang, Y., Materials and Mechanics for Stretchable Electronics. *Science* **2010,** *327*, 1603-1607.

(36) Tang, Y.; Li, Y.; Hong, Y.; Yang, S.; Yin, J., Programmable active kirigami metasheets with more freedom of actuation. *Proc. Natl. Acad. Sci. U. S. A.* **2019,** *116*, 26407-26413.

(37) Ke, Y.; Yin, Y.; Zhang, Q.; Tan, Y.; Hu, P.; Wang, S.; Tang, Y.; Zhou, Y.; Wen, X.; Wu, S.; White, T. J.; Yin, J.; Peng, J.; Xiong, Q.; Zhao, D.; Long, Y., Adaptive Thermochromic Windows from Active Plasmonic Elastomers. *Joule* **2019,** *3*, 858-871.

(38) Ke, Y.; Zhang, Q.; Wang, T.; Wang, S.; Li, N.; Lin, G.; Liu, X.; Dai, Z.; Yan, J.; Yin, J.; Magdassi, S.; Zhao, D.; Long, Y., Cephalopod-inspired versatile design based on plasmonic VO2 nanoparticle for energy-efficient mechano-thermochromic windows. *Nano Energy* **2020,** *73*, 104785.

(39) Jiang, H.; Khang, D.-Y.; Song, J.; Sun, Y.; Huang, Y.; Rogers, J. A., Finite deformation mechanics in buckled thin films on compliant supports. *Proc. Natl. Acad. Sci. U. S. A.* **2007,** *104*, 15607-15612.

(40) Chan, J. Y. E.; Ruan, Q.; Wang, H.; Wang, H.; Liu, H.; Yan, Z.; Qiu, C.-W.; Yang, J. K. W., Full Geometric Control of Hidden Color Information in Diffraction Gratings under Angled White Light Illumination. *Nano Lett.* **2022,** *22*, 8189-8195.

(41) Görrn, P.; Wagner, S., Topographies of plasma-hardened surfaces of poly(dimethylsiloxane). *J. Appl. Phys.* **2010,** *108*, 093522.

(42) Qin, D.; Xia, Y.; Whitesides, G. M., Soft lithography for micro- and nanoscale patterning. *Nat. Protocols* **2010,** *5*, 491-502.

(43) Mazurek, P.; Vudayagiri, S.; Skov, A. L., How to tailor flexible silicone elastomers with mechanical integrity: a tutorial review. *Chem. Soc. Rev.* **2019,** *48*, 1448-1464.

(44) Qi, D.; Zhang, K.; Tian, G.; Jiang, B.; Huang, Y., Stretchable Electronics Based on PDMS Substrates. *Adv. Mater.* **2021,** *33* , 2003155.